

Supporting Information

AB-Side Growth Strategy: A New Approach to Regulate Electrocatalytic Performance of Metal-Organic Framework Composite Materials

Jing Ye, ‡ Ning Chai, ‡ Qingqing Guo, Tianyu Chen, Wei wang, Yun Hu, Fang Han,
Fei-Yan Yi* and Xinghu Ma*

School of Materials Science and Chemical Engineering, Ningbo University, Ningbo,
Zhejiang, 315211, P. R. China, E-mail: yifeiyan@nbu.edu.cn, maxinghua@nbu.edu.cn

Table of contents

1. Experimental Section.....	S3
1.1 General Information.....	S3
1.2 Preparation of Ni foams (NFs).....	S3
1.3 Synthesis of FeCo-MOF-74/NF.....	S3
1.4 Synthesis of ZIF-67/NF.....	S3
1.5 Synthesis of FeCo-MOF-74/NF/ZIF-67 ((A)MOF/NF/ZIF(B)) and FeCo-MOF-74/ZIF-67/NF ((A)ZIF/MOF/NF).....	S4
1.6 Synthesis of FeCo-MOF-74@ZIF-67/NF ((A)MOF@ZIF/NF).....	S4
1.7 Prepared of IrO ₂ /NF and Pt/C/NF.....	S4
1.8 Electrochemical Test.....	S4
2. Supplementary Data.....	S5
3. References.....	S15

1.1 General Information

All chemical reagents were analytically pure, including cobaltous nitrate hexahydrate ($\text{Co}(\text{NO}_3)_2 \cdot 6\text{H}_2\text{O}$), ferrous(II) chloride tetrahydrate ($\text{FeCl}_2 \cdot 4\text{H}_2\text{O}$), 2-methylimidazole (2-MIM, $\text{C}_4\text{H}_6\text{N}_2$), 2,5-dihydroxyterephthalic acid (DOBDC), N,N-dimethylformamide (DMF), anhydrous ethanol ($\text{C}_2\text{H}_6\text{O}$), hydrochloric acid (HCl) and Potassium hydroxide (KOH). Commercial nickel foam (NF) (thickness: 1.7 mm), Nafion solution (5 wt%), Pt/C (20 wt%), and commercial IrO_2 catalyst were obtained from Sigma-Aldrich Crop.

X-ray diffraction (XRD) data for all materials were collected using a Bruker D8 Advance diffractometer with Cu $\text{K}\alpha$ radiation in the 2θ range of 5° to 50° . Scanning electron microscopy (SEM) images and energy-dispersive X-ray spectroscopy (EDX) were obtained using a FEI Nova Nano SEM 450. X-ray photoelectron spectroscopy (XPS) measurements were conducted with a Thermo Scientific K-Alpha instrument to assess the chemical valence states.

1.2 Preparation of Ni foams (NFs)

Initially, nickel foams (NFs) with dimensions of $3 \times 2 \text{ cm}^2$ were cleaned by ultrasonication in a 3 M hydrochloric acid (HCl) solution for 15 minutes to remove the oxide layers from the surface. Then, the NFs were washed with alcohol and water for 30 min under ultrasonication, respectively. Finally, it dried in the vacuum oven at 60°C for 12 h.

1.3 Synthesis of FeCo-MOF-74/NF

Typically, 0.18 mmol of $\text{Co}(\text{NO}_3)_2 \cdot 6\text{H}_2\text{O}$, 0.18 mmol of $\text{FeCl}_2 \cdot 4\text{H}_2\text{O}$, and 0.50 mmol of DOBDC (2,5-dihydroxyterephthalic acid) were dissolved in 7.5 mL of a mixed solvent composed of DMF, ethanol, and water ($v/v/v = 1:1:1$). The mixture was then subjected to ultrasonication for 20 minutes at room temperature to achieve a homogeneous dispersion. The resulting solution was transferred into a 50 mL Teflon-lined stainless-steel autoclave, followed by the addition of the pre-treated nickel foam. The autoclave was then heated to 120°C for 24 hours.

1.4 Synthesis of ZIF-67/NF

5 mmol of $\text{Co}(\text{NO}_3)_2 \cdot 6\text{H}_2\text{O}$ were dissolved in 40 mL of methanol and stirred to form a homogeneous solution (Solution A), to which a piece of pre-treated nickel foam was added. Subsequently, 7 mmol of 2-MIM was dissolved in 40 mL of methanol to form Solution B, which was then rapidly added to Solution A under continuous stirring. The resulting mixed solution was allowed to stand for 6 hours at room temperature.

1.5 Synthesis of FeCo-MOF-74/NF/ZIF-67 ((A)MOF/NF/ZIF(B)) and FeCo-MOF-74/ZIF-67/NF ((A)ZIF/MOF/NF)

5 mmol of $\text{Co}(\text{NO}_3)_2 \cdot 6\text{H}_2\text{O}$ were dissolved in 40 mL of methanol and stirred to form a uniform solution (Solution A), into which a piece of FeCo-MOF-74/NF was immersed. Subsequently, 7 mmol of 2-MIM was dissolved in 40 mL of methanol to form Solution B, which was then rapidly added to Solution A under stirring. The mixture was allowed to react for 6 hours. If ZIF-67 and FeCo-MOF-74 grow on the same side of the foam, the resulting material is denoted as (A)ZIF/MOF/NF. If ZIF-67 and MOF-74 grow on both sides, the material is referred to as (A)MOF/NF/ZIF(B).

1.6 Synthesis of FeCo-MOF-74@ZIF-67/NF ((A)MOF@ZIF/NF)

7 mmol of 2-MIM, as the organic ligand, was dissolved in 40 mL of methanol to form a solution. A piece of FeCo-MOF-74/NF was then immersed in the solution at room temperature for durations of 3, 6, 12, and 24 hours. After the reaction, the FeCo-MOF-74@ZIF-67/NF composites were thoroughly washed with ethanol and dried in an oven at 60 °C for 24 hours.

1.7 Prepared of IrO_2 /NF and Pt/C/NF

10 mg of IrO_2 or Pt catalyst were first dispersed in 470 μL of ethanol, along with 30 μL of Nafion solution, and subjected to ultrasonic treatment for 30 minutes to form a homogeneous ink. Subsequently, 100 μL of the prepared ink was slowly dripped onto a $1 \times 1 \text{ cm}^2$ nickel foam (NF) and allowed to dry in air.

1.8 Electrochemical Test

The electrochemical test was carried out at an electrochemical workstation (CHI 760E, Chen Hua, China) using a three-electrode system with 1.0 M KOH.¹ The sample modified NF electrode, Ag/AgCl electrode, and carbon rod were used as the working, reference, and counter electrodes, respectively. The Ag/AgCl reference electrode was calibrated against the reversible hydrogen electrode (RHE), where $E_{\text{RHE}} = E_{\text{Ag/AgCl}} + 0.197 + 0.059 \times \text{pH}$. Polarization curves were measured using linear sweep voltammetry (LSV) at a scan rate of 5 mV/s.² All the data were recorded with 85% iR compensation. Tafel plots were obtained from the extrapolation of the linear region of a plot of the overpotential versus current density. Cyclic voltammetry (CV) was tested in the range from 0 V to 0.1 V using different scan speeds (20, 40, 60, 80, 100 and 120 mV/s).³ Electrochemical impedance spectroscopy (EIS) was carried out at different overpotential (vs. RHE) over the frequency spectrum range from 100 kHz to 10 Hz at the amplitude of the sinusoidal voltage of 5 mV and it performed at 0.577 V (vs RHE) for the OER and -1.23 V (vs RHE) for the HER.⁴ The chronopotentiometry (CP) test were conducted the potential at a current density of 10 mA cm^{-2} to assess the electrochemical stability of the catalysts.⁵

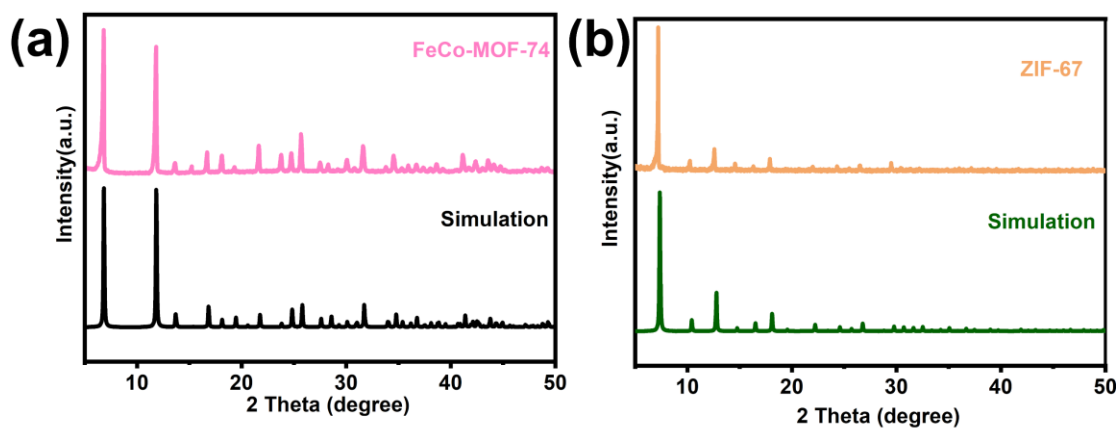


Fig. S1 XRD pattern of (a) FeCo-MOF-74 and simulated one (CCDC no. 1494751) (b) ZIF-67 and simulation one (CCDC no. 671073).

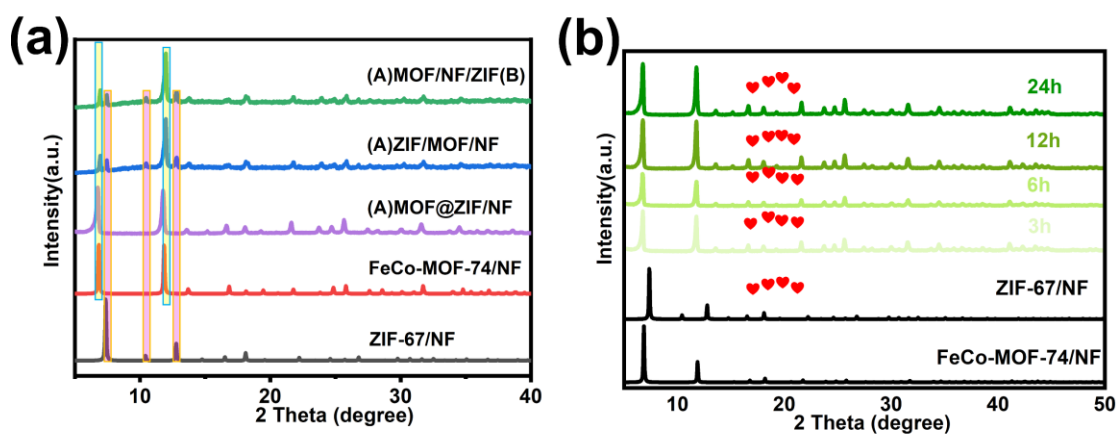


Fig. S2 (a) XRD pattern of (A)MOF/NF/ZIF(B), (A)ZIF/MOF/NF and (A)MOF@ZIF/NF (b)XRD pattern of the (A)MOF@ZIF/NF with the different time.

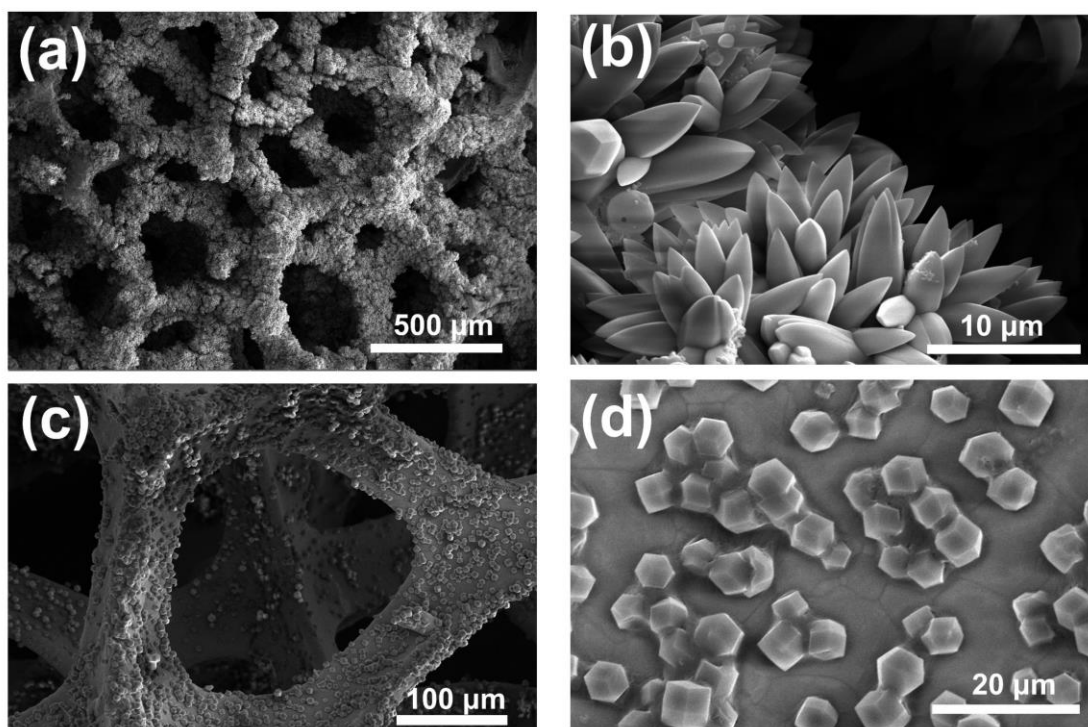


Fig. S3 SEM images of (a, b) FeCo-MOF-74/NF (c, d) ZIF-67.

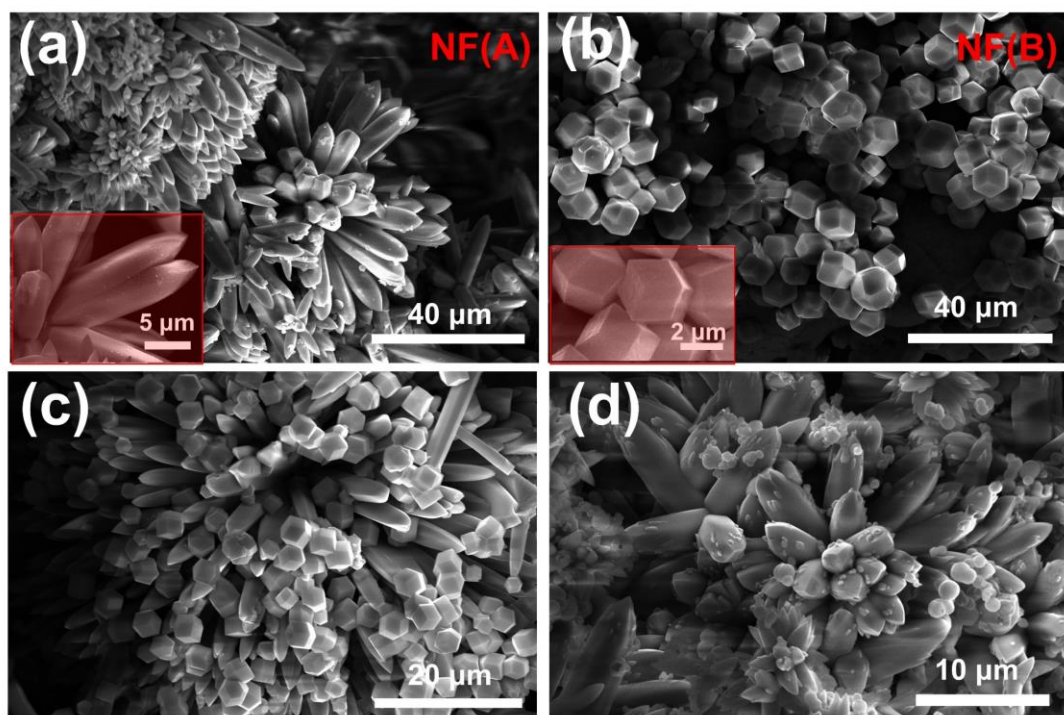


Fig. S4 SEM images of (A)MOF/NF/ZIF(B) (a) nickel foam for A (b) nickel foam for B; (c) SEM images of (A)ZIF/MOF/NF; (d) SEM images of (A)MOF@ZIF/NF.

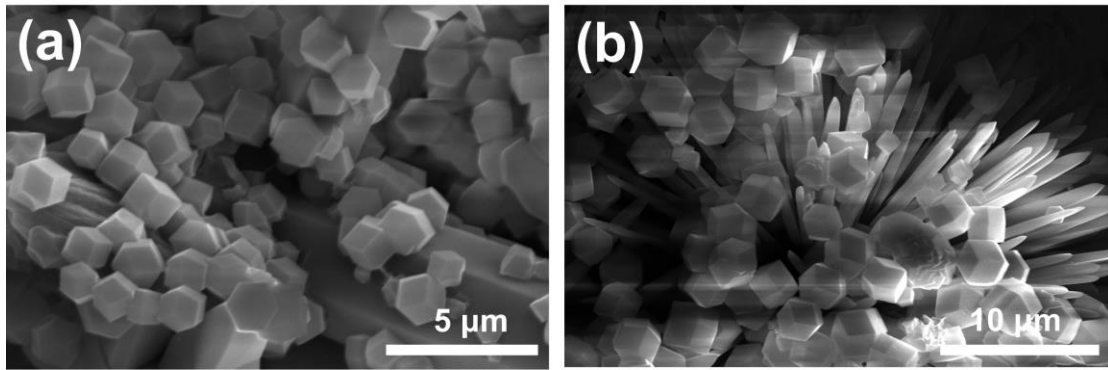


Fig. S5 SEM images of (A)ZIF/MOF/NF.

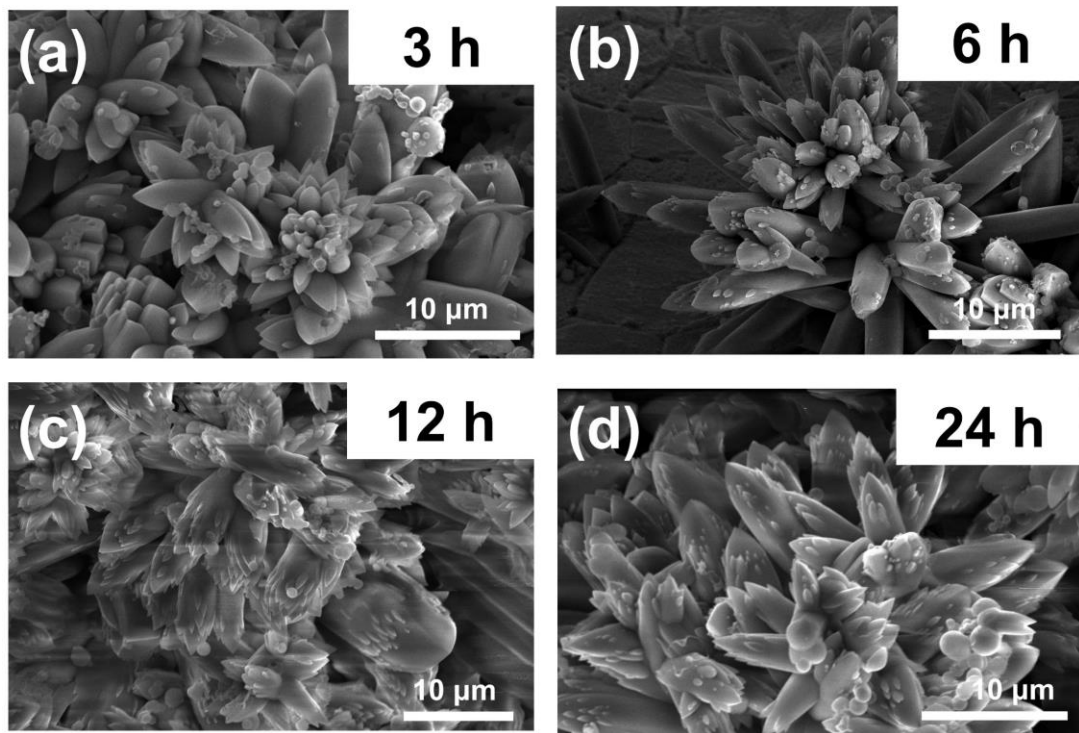


Fig. S6 SEM images of (A)MOF@ZIF/NF with different time.

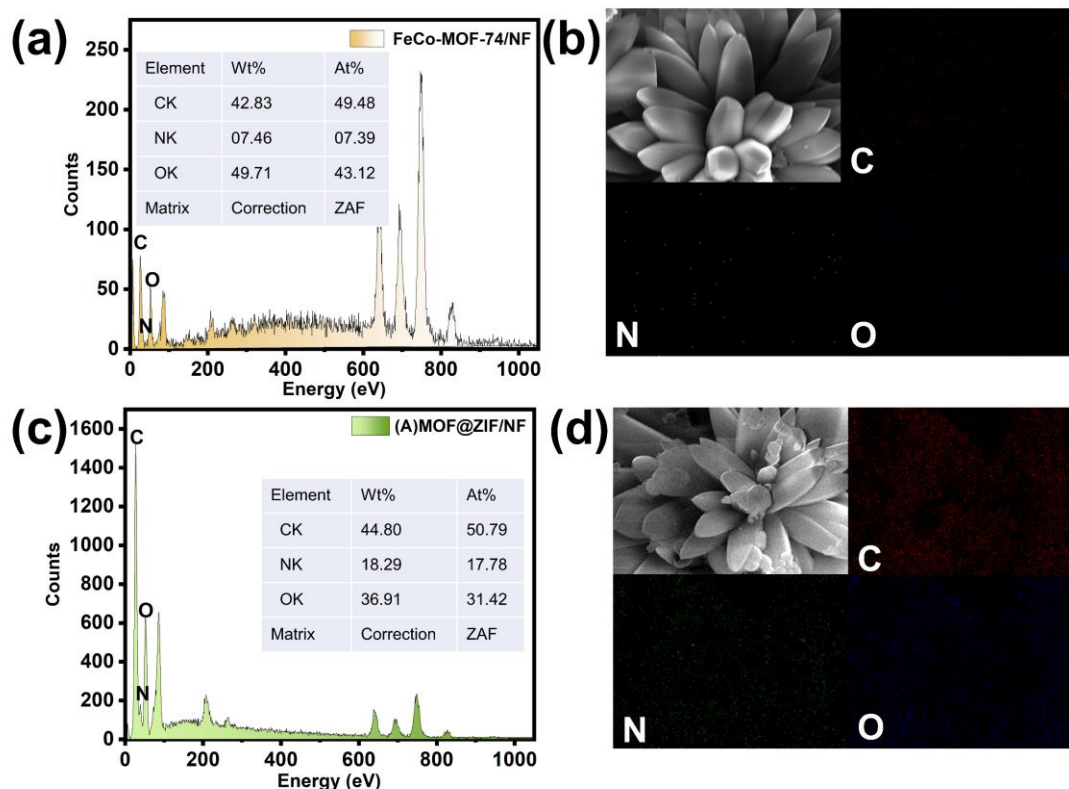


Fig. S7 (a) EDX spectrum of FeCo-MOF-74 (b) elemental mapping of FeCo-MOF-74 (c) EDX spectrum of (A)MOF@ZIF/NF. (d) elemental mapping of (A)MOF@ZIF/NF.

Table S1. Comparison of OER electrocatalytic performance between as-synthesized composite materials in this work and other relative MOF based catalysts

Catalyst	Overpotential (mV@mA cm ⁻²)	Electrolyte	Ref
Er _{0.4} Fe-MOF/NF	248@100	1.0 M KOH	6
FeNiZnS-1	249@10	1.0 M KOH	7
Co-MOF-D5	300@10	1.0 M KOH	8
B-MOF-Zn-Co	362@100	1.0 M KOH	9
NiFe-MOF/IF	262@100	1.0 M KOH	10
Fe-NiCo-MOF/NF	290@50	1.0 M KOH	11
NiCo-MOF/NF	270@50	1.0 M KOH	12
NiCo-TDC-MOF	248@100	1.0 M KOH	13
MFN-MOFs(2:1)/NF	235@50	1.0 M KOH	14
Au-MOF-74/MIL-53	218@50	1.0 M KOH	15
NiFe LDH/MOF@MXene	171@10	1.0 M KOH	16
Mo _{4g} ZIF-67	221@10	1.0 M KOH	17

MXene/MIL Fe-53	292@50	1.0 M KOH	18
(A)MOF@ZIF/NF	188@50	1.0 M KOH	This work
(A)ZIF/MOF/NF	208@50	1.0 M KOH	This work
(A)MOF/NF/ZIF(B)	203@50	1.0 M KOH	This work

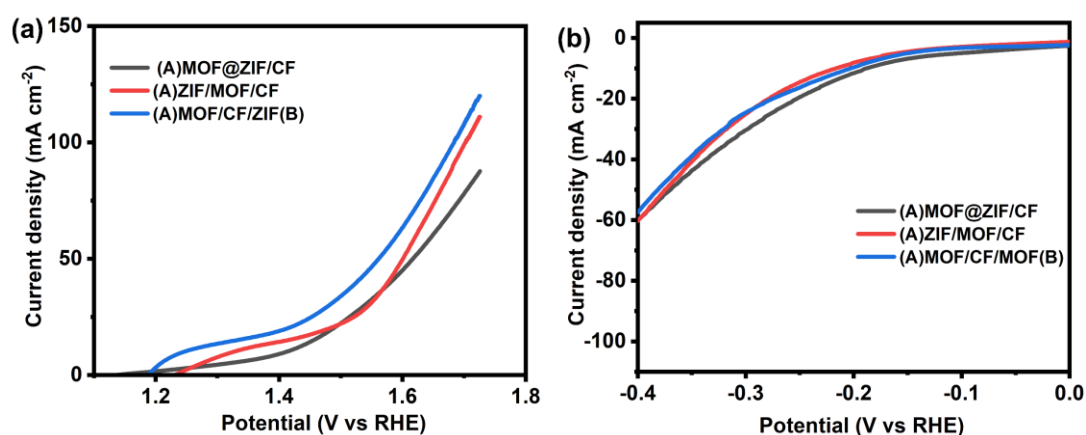


Fig. S8 (a) OER polarization, and (b) HER polarization of (A)MOF@ZIF/CF, (A)ZIF/MOF/CF and (A)MOF/CF/ZIF(B) in 0.1 M KOH.

Table S2. OER and HER electrocatalytic performance of (A)MOF@ZIF/CF, (A)ZIF/MOF/CF and (A)MOF/CF/ZIF(B)

Catalyst	OER	HER
	Overpotential (mV@mA cm ⁻²)	Overpotential (mV@mA cm ⁻²)
(A)MOF@ZIF/CF	385@50	188@10
(A)ZIF/MOF/CF	370@50	215@10
(A)MOF/CF/ZIF(B)	331@50	204@10

To further evaluate the influence of different conductive substrates on electrocatalytic performance of the composite materials, we selected other substrates for comparison, including carbon cloth (CC) and copper foam (CF). When CC was used as the substrate, the target composite materials could not be successfully synthesized, primarily due to the soft and flexible nature of CC, which makes it challenging to achieve uniform and stable growth on both AB sides. In contrast, CF, with its superior mechanical strength and three-dimensional porous structure, provided robust support for the AB-side growth strategy, enabling the successful construction of the corresponding composites, denoted as (A)MOF@ZIF/CF, (A)ZIF/MOF/CF, and (A)MOF/CF/ZIF(B). Subsequently, the OER electrocatalytic performance of these CF-based composites was evaluated. As shown in Fig. S8 and Table S2, (A)MOF@ZIF/CF requires an overpotential of 385 mV to achieve a current density of 50 mA cm⁻², (A)ZIF/MOF/CF requires 370 mV, and (A)MOF/CF/ZIF(B) requires 331 mV. These values are significantly higher than those

of the corresponding composites synthesized on NF, indicating inferior catalytic performance when CF is used as the substrate. During the HER process, (A)MOF@ZIF/CF requires an overpotential of 188 mV to reach 10 mA cm^{-2} , while (A)ZIF/MOF/CF and (A)MOF/CF/ZIF(B) require 215 mV and 204 mV, respectively. Although (A)MOF@ZIF/CF exhibits the lowest overpotential at 10 mA cm^{-2} compared to the NF-based composites, the difference in overpotential is minimal. Overall, these results indicate that NF is a more suitable conductive substrate, offering superior electrocatalytic activity. Therefore, NF is recommended as the preferred substrate for further studies.

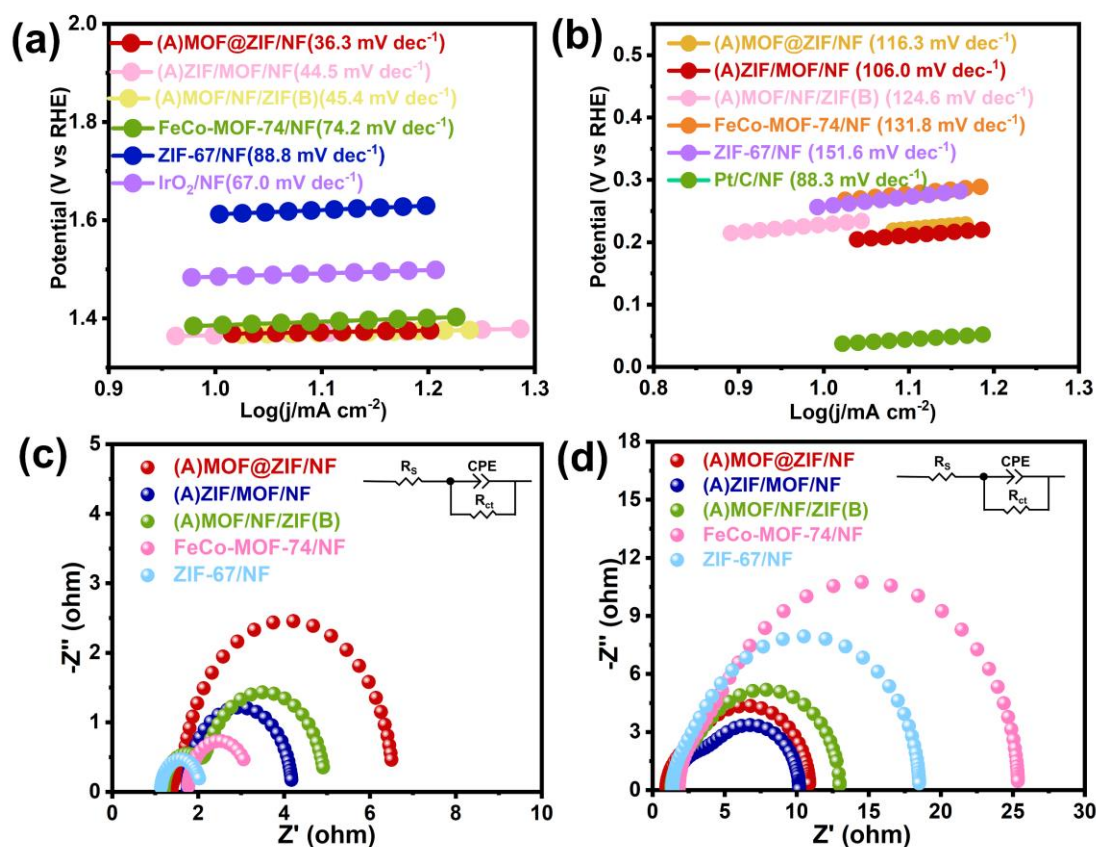


Fig. S9 (a) The corresponding Tafel plots to OER (b) The corresponding Tafel plots to HER (c) Nyquist EIS plots for OER (d) Nyquist EIS plots for HER.

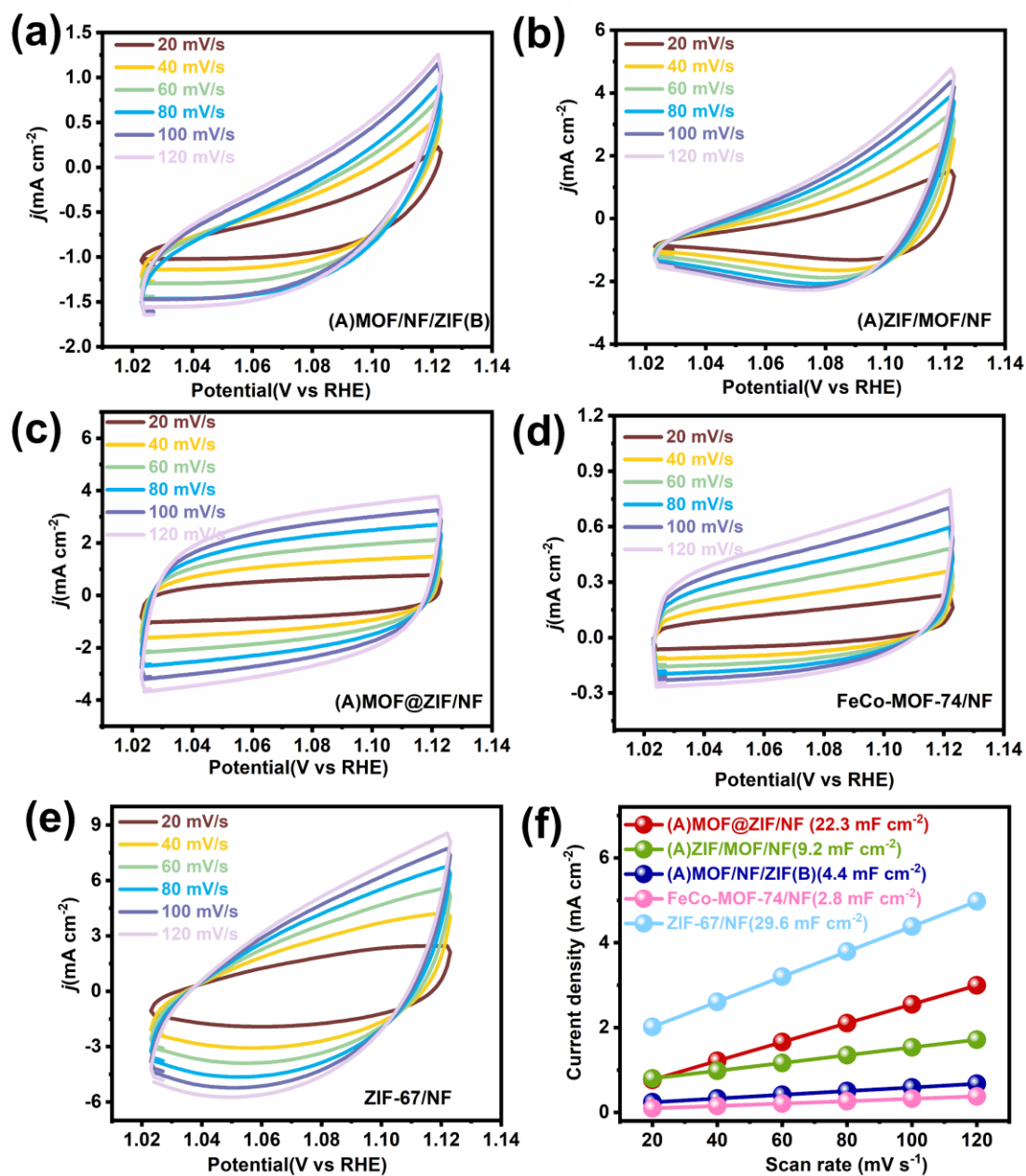


Fig. S10 CV curves at various scan rates: (a) (A)MOF/NF/ZIF(B), (b) (A)ZIF/MOF/NF, (c) (A)MOF@ZIF/NF, (d) FeCo-MOF-74, (e) ZIF-67/NF, (f) C_{dl} data of Nyquist plots.

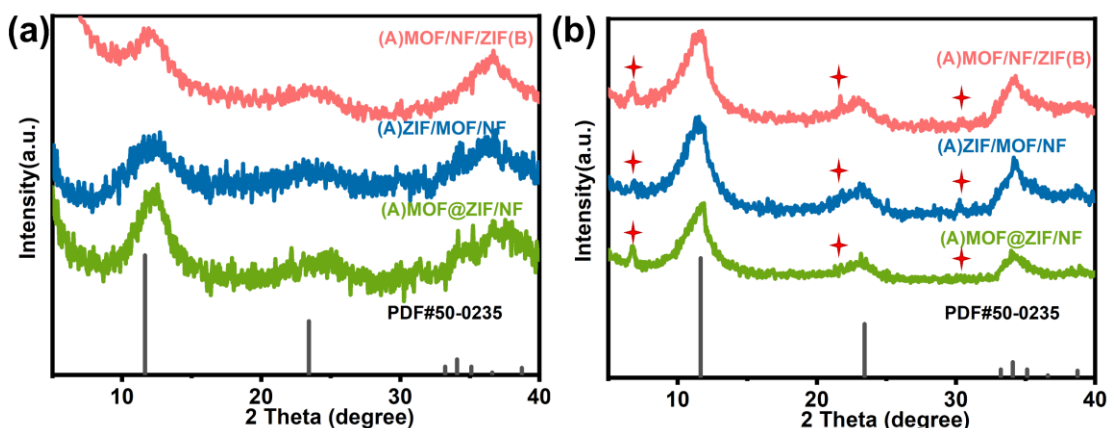


Fig. S11 XRD patterns of the (A)MOF@ZIF/NF, (A)ZIF/MOF/NF, and (A)MOF/NF/ZIF(B) after the (a) OER and (b) HER for 12 h electrolysis process.

XRD spectra in Fig. S11 show that only broad characteristic peaks can be observed for all electrode materials after OER and HER tests, where the peaks located at 11.6°, 22.4°, 36.6°, and 38.7° correspond to the (003), (006), (104), and (015) crystal faces of $\text{Co}_{5.84}\text{Fe}_{2.16}(\text{OH})_{16}(\text{CO}_3)_{1.08} \cdot 0.32(\text{H}_2\text{O})$ (JCPDS No. 050-0235), respectively.^{19, 20} In other words, their MOF frameworks of the three composite materials have transformed into metal hydroxides during the OER and HER processes, which is likely the actual catalytic active center.^{21, 22} This is a widely observed phenomenon for MOF electrode materials. In contrast to OER process, some weak diffraction peaks at 6.74°, 21.75°, and 30.37° after the HER stability test still can be observed, that is accordance with a characteristic peak of the original MOF, implying that MOF skeleton may be intact under HER condition.

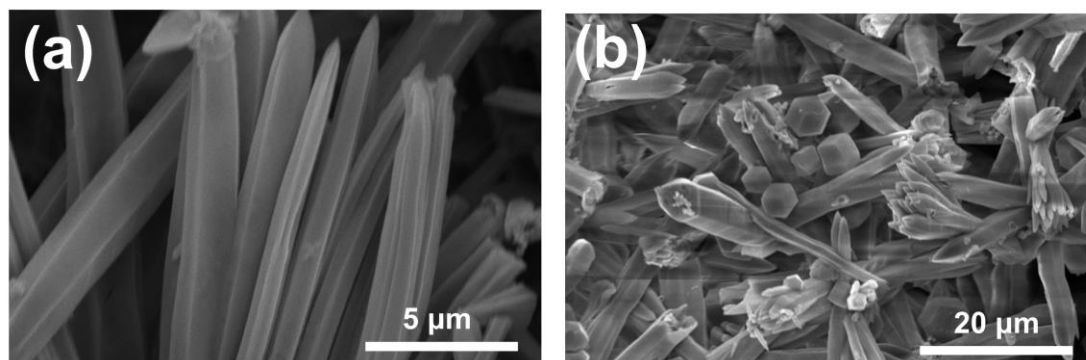


Fig. S12 SEM images of (a) (A)MOF@ZIF/NF after the OER test, and (b) (A)ZIF/MOF/NF after the HER test.

SEM images in Fig. S12 reveal the morphological changes of (A)MOF@ZIF/NF after OER testing and (A)ZIF/MOF/NF after HER testing. After the OER test, the overall nanoflower morphology in the structure of (A)MOF@ZIF/NF can be still observed, just, the surface of nanoflower becomes smooth, and the small particles originally distributed on the nanoflower structures disappear, suggesting possible surface reconstruction during the electrochemical oxidation process. Parallel examination of the HER-tested (A)ZIF/MOF/NF in Fig. S12b demonstrates partial preservation of

both components: the FeCo-MOF-74 nanoflower framework remains detectable, while only residual ZIF dodecahedral structures are observable on the MOF surfaces, indicating preferential dissolution or morphological transformation of the ZIF phase during reduction.

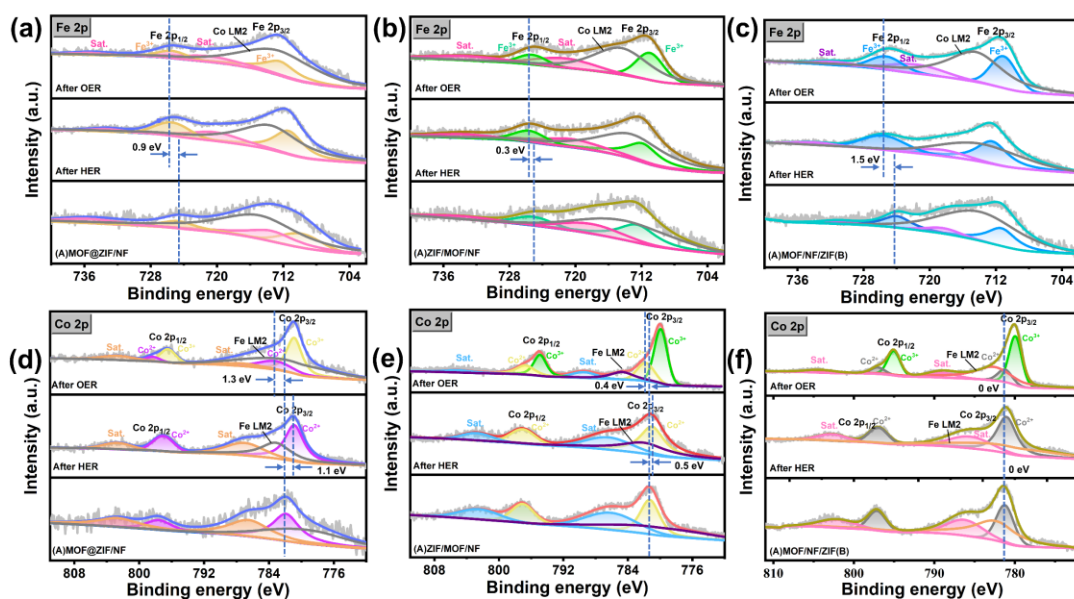


Fig. S13 XPS spectra of Fe 2p before and after HER and OER test for (a) (A)MOF@ZIF/NF, (b) (A)ZIF/MOF/NF and (c) (A)MOF/NF/ZIF(B); XPS spectra of Co 2p before and after HER and OER test for (d) (A)MOF@ZIF/NF, (e) (A)ZIF/MOF/NF and (f) (A)MOF/NF/ZIF(B).

Fig. S13 presents high-resolution Fe 2p and Co 2p XPS spectra for (A)MOF@ZIF/NF, (A)ZIF/MOF/NF, and (A)MOF/NF/ZIF(B) before and after HER/OER stability tests. All materials exhibit characteristic Fe 2p_{3/2} and Fe 2p_{1/2} peaks with satellite features, along with Co LM2 Auger peaks in the Fe 2p region. For (A)MOF@ZIF/NF, the Fe³⁺ 2p_{3/2} and 2p_{1/2} peaks appear at 710.0 eV and 724.8 eV respectively, with satellite peaks at 713.6 eV and 734.9 eV.²³ Post-reaction analysis reveals positive binding energy shifts of ~0.9 eV (Fe 2p_{1/2} in (A)MOF@ZIF/NF), ~0.3 eV ((A)ZIF/MOF/NF), and 1.5 eV ((A)MOF/NF/ZIF(B)), indicating modified Fe electronic environments and enhanced binding strength. The Co 2p spectra (Figs. S13d-f) consistently show Co 2p_{3/2}, Co 2p_{1/2}, satellite peaks, and Fe LM2 Auger features, confirming strong Fe-Co electronic coupling. In (A)MOF@ZIF/NF, Co²⁺ peaks at 781.9 eV (2p_{3/2}) and 797.7 eV (2p_{1/2}) undergo a 1.1 eV negative shift after HER testing, while OER testing induces a 1.3 eV positive shift and emergence of new Co³⁺ peaks (780.9 eV and 796.4 eV).^{24, 25} Similar redox behavior is observed for (A)ZIF/MOF/NF, though with small shifts (~0.5 eV negative after HER, ~0.4 eV positive after OER). (A)MOF/NF/ZIF(B) shows minimal binding energy changes but develops new Co³⁺ features at 779.0 eV and 795.0 eV. Post-OER increasing Fe³⁺/Fe²⁺ area ratios of 3.5, 2.4, and 2.2 for (A)MOF@ZIF/NF, (A)ZIF/MOF/NF, and (A)MOF/NF/ZIF(B) respectively confirm substantial surface cobalt oxidation during OER conditions.²⁶

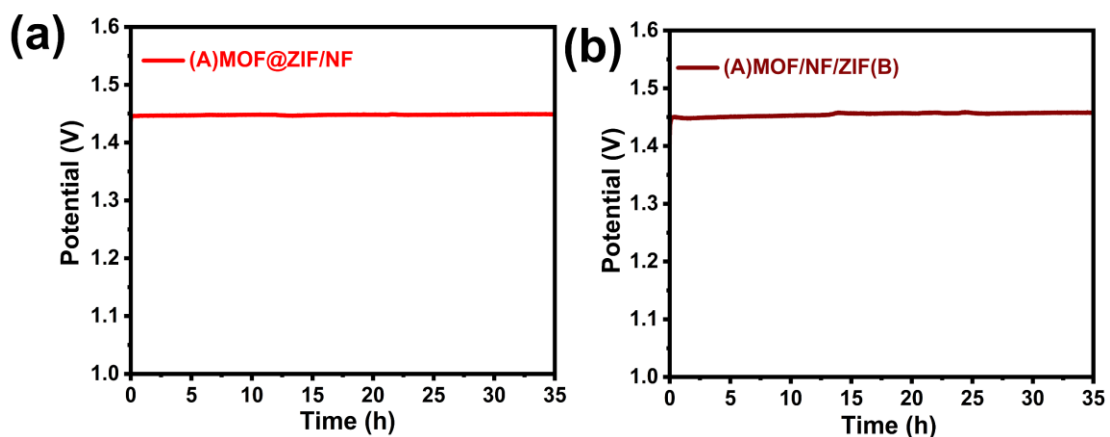


Fig. S14 OER results of Chronopotentiometry curve for (a) (A)MOF@ZIF/NF (b) (A)MOF/NF/ZIF(B) at a constant current density of 10 mA cm^{-2} .

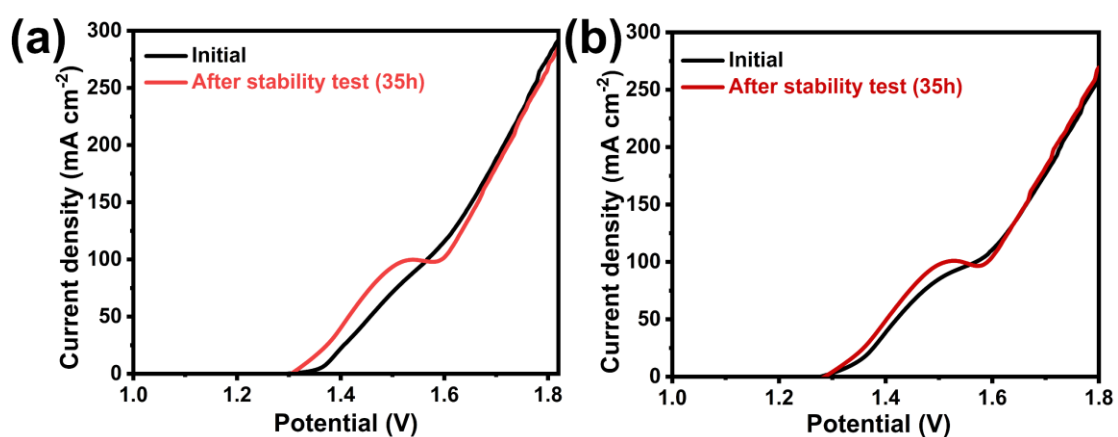


Fig. S15 (a) Polarization curves of (A)MOF@ZIF/NF before and after stability OER test. (b) Inset: Polarization curves of (A)MOF/NF/ZIF(B) before and after OER test.

References

1. Y. Zhang, *et al.*, *Chin. J. Struct. Chem.*, 2024, **43**, 100243.
2. Y. Guo, *et al.*, *Chin. J. Struct. Chem.*, 2024, **43**, 100206.
3. N. Baby, *et al.*, *Int. J. Hydrogen Energy*, 2025, **130**, 127-138.
4. S. Yu, *et al.*, *Coord. Chem. Rev.*, 2025, **520**, 216144.
5. H. Guan, *et al.*, *Colloids Surf. A Physicochem. Eng. Asp.*, 2021, **624**, 126596.
6. Y. Ma, *et al.*, *Nanomaterials*, 2021, **11**, 1847.
7. T. Liu, *et al.*, *Inorg. Chem. Front.*, 2024, **11**, 6064-6071.
8. T. Ni, *et al.*, *Chin. J. Struct. Chem.*, 2024, **43**, 100210.
9. X. Lin, *et al.*, *Small*, 2023, **20**, 2308517.
10. Y. Zhang, *et al.*, *Dalton Trans.*, 2021, **50**, 4720-4726.
11. T. Sun, *et al.*, *CrystEngComm*, 2021, **23**, 7650-7657.
12. P. Thangasamy, *et al.*, *Nanoscale Adv.*, 2020, **2**, 2073-2079.
13. M. Salman, *et al.*, *J. Power Sources*, 2025, **629**, 235942.
14. D. Senthil Raja, *et al.*, *Nano Energy*, 2019, **57**, 1-13.
15. X. Liu, *et al.*, *Int. J. Hydrogen Energy*, 2024, **69**, 441-450.
16. J. Jiang, *et al.*, *ACS Catal.*, 2025, **15**, 2561-2575.
17. M. Zahra, *et al.*, *Int. J. Hydrogen Energy*, 2024, **89**, 310-319.
18. K. Farooq, *et al.*, *Nanoscale Adv.*, 2025, **7**, 1561-1571.
19. J. Zhao, *et al.*, *ChemElectroChem*, 2020, **7**, 2309-2313.
20. Y. Q. Jin, *et al.*, *J. Power Sources*, 2018, **402**, 388-393.
21. J. Ding, *et al.*, *Appl. Catal. B Environ.*, 2021, **292**, 120174.
22. H. Sun, *et al.*, *Adv. Mater.*, 2020, **32**, 2006784.
23. X. Zhang, *et al.*, *Chin. J. Struct. Chem.*, 2024, **43**, 100200.
24. L. Xiao, *et al.*, *Fuel*, 2025, **381**, 133516.
25. K. Wang, *et al.*, *Chin. J. Struct. Chem.*, 2024, **42**, 100104.
26. J. Jiang, *et al.*, *ACS Catal.*, 2025, **15**, 2561-2575.